Copper(II) and Zn(II) coordination chemistry of tetraaza[*n*]cyclophanes

Martin Chadim,[a] Pilar Díaz,[b] Enrique García-España,*[b] Jana Hodacova,*[a] Peter C. Junk,[d] Julio Latorre,[b] José M. Llinares,[c] Conxa Soriano[c] and Jiri Zavada[a]

[a] *Institute of Organic Chemistry and Biochemistry, Academy of Sciences of the Czech Republic, Flemingovo nam. 2, 166 10 Prague 6, Czech Republic. E-mail: hodacova@uochb.cas.cz*
[b] *Departamento de Química Inorgánica, Instituto de Ciencia Molecular, Universidad de Valencia, C/ Dr. Moliner 50, 46100 Burjassot (Valencia), Spain. E-mail: enrique.garcia-es@uv.es.*
[c] *Departamento de Química Orgánica, Instituto de Ciencia Molecular, Universidad de Valencia, Avda. Vicente Andrés Estellés, s/n, 46100 Burjassot (Valencia), Spain*
[d] *School of Chemistry, PO Box 23, Monash University, Victoria, 3800, Australia. E-mail: peter.junk@sci.monash.edu.au.*

Received* (*in in London, UK*) *27th March 2003, Accepted 13th May 2003
First published as an Advance Article on the web 12th June 2003

The acid–base behaviour and Zn^{2+} and Cu^{2+} metal coordination chemistry of the novel orthocyclophane ligands 2,5,8,11-tetraaza[12]orthocyclophane (**L²**) and 2,5,9,12-tetraaza[13]orthocyclophane (**L³**) and metacyclophane 2,5,8,11-tetraaza[12]metacylophane (**L¹**) are studied. Important differences in the chemistry of these compounds are found depending on the substitution of the aromatic ring. The ortho derivatives are much more basic in their first two protonation steps while the metacyclophane presents much larger constants in the third and fourth protonation stages. The crystal structure of the picrate salt of $[H_2\mathbf{L^3}]^{2+}$ shows an alternate disposition of the protons in the molecule with formation of N–$H^+\cdots$N hydrogen bonds between the protonated and non-protonated amino groups. While formation of mononuclear Cu^{2+} complexes is observed for **L²** and **L³**, the metaderivative **L¹** forms also binuclear Cu^{2+} species which predominate largely for molar ratios M:L 2:1. The crystal structure of the complex $[Cu\mathbf{L^3}Cl](ClO_4)$ shows a chain-like arrangement with the $[Cu\mathbf{L^3}]^{2+}$ units interconnected by chlorine atoms. The coordination geometry around the metal ion is a distorted octahedron with the nitrogen atoms of the macrocycle at the vertices of the equatorial plane and chloride anions asymmetrically disposed at the axial positions. The Zn^{2+} complexes of the ortho derivatives **L²** and **L³** are also much more stable than the meta counterparts. The crystal structure of $[Zn\mathbf{L^3}Cl]Cl{\cdot}H_2O$ shows a square pyramidal geometry with the nitrogen atoms of the macrocycle at the vertices of the equatorial plane and one chloride anion occupying the axial position. In this case there are not chain arrangements. The involvement of all the nitrogen atoms in the coordination of Zn^{2+} by **L³** in aqueous solution is proved by ^{1}H and ^{13}C NMR.

Introduction

A recurrent feature in the active site of many metalloenzymes is that they offer to the metal ions coordinatively unsaturated environments so that the metal can fix through its vacant positions a given substrate inducing its transformation. Additionally, a number of these metalloenzymes present binuclear sites in which the two metal ions cooperate in the recognition and activation of a given substrate.[1]

This knowledge from the biological world has prompted many researchers to synthesize molecules displaying such characteristics and several approaches have been used. Some of these molecules could be: i) mononuclear complexes interconnected by bridging ligands, ii) ditopic ligands with well-separated and identifiable binding sites, iii) macrocycles containing a large number of donor groups in the cavity.[2]

A much more novel strategy consists of generating cyclic compounds with a reduced number of donors, in which the binucleating ability is the result of a correct balance between electron and stereochemical requirements. One such example is the macrocycle 2,5,8,11-tetraaza[12]paracyclophane in which both ends of a triethylenetetramine chain are linked in para position through benzylic groups to a benzene ring (**L**).[3] In such a ligand, on the one hand the presence of the para-substituted ring prevents the simultaneous coordination of both benzylic nitrogens to a single metal ion, and on the other hand the size of the polyamine makes the bridge rigid enough to divide it into two separated coordination sites This situation was evidenced by the crystal structure of the binuclear Cu^{2+} complex of **L**,[3] $[Cu_2\mathbf{L}Cl_2]Cl_2$, in which the tetraamine chain behaves as two independent ethylenediame subunits each one of them coordinating a Cu^{2+} metal ion. Larger more flexible chains would not offer this characteristic.[4]

In order to complete this picture and understand the effects of the different substitution of the benzene spacer, macrocycles with orthophenylene and methaphenylene units needed to be analyzed. In the present work we report on the synthesis of the new metacyclophane 2,5,8,11-tetraaza[12]metacyclophane (**L¹**), which is analogous to **L** but with the benzene ring meta-substituted. We report on its protonation behaviour and its coordination capabilities towards Cu^{2+} and Zn^{2+}. We present the same studies for the recently prepared compounds 2,5,8,11-tetraaza[12]orthocyclophane (**L²**), the ortho counterpart of **L**

 DOI: 10.1039/b303470d

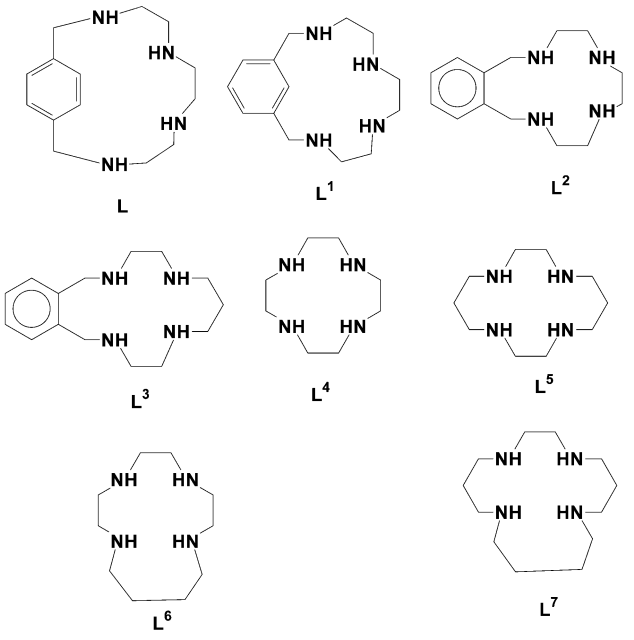

Chart 1

and $\mathbf{L^1}$, and 2,5,9,12-tetraaza[13]orthocyclophane ($\mathbf{L^3}$). Additionally, we describe the crystal structure of the complexes $[Cu\mathbf{L^3}Cl](ClO_4)$ and $[Zn\mathbf{L^3}Cl]Cl{\cdot}H_2O$.

Experimental

Synthesis of $\mathbf{L^1}\cdot 4HBr$

The procedure used was a modification of that previously described for related para- and metacyclophane derivatives.[5,6]

$\mathbf{L^1}\cdot 4Ts$

The pertosylated tetraamine trien $\mathbf{L^1}$ (5.0 g, 6.6 mmol),[6] and K_2CO_3(4.4 g. 31.6 mmol) were suspended in refluxing DMF (100 mL). To this mixture, a solution of 1,3-bis(bromomethyl)-benzene (1.8 g, 6.8 mmol) in 100 mL of DMF was added dropwise over a period of 4 h. After the addition was completed, the reaction was kept refluxing for 48 h. The solution was vacuum evaporated to dryness to obtain the crude product that was recrystalised in CH_2Cl_2/EtOH to give the final product (5.3 g, 93% yield): mp 228–230. ^{1}H NMR, 2.44 (s, 6H), 2.46 (s, 6H), 2.67 (s, 4H), 2.90–2.99 (m, 8H), 4.12 (s, 4H), 7.28–7.38 (m, 12 H), (7.66–7.76 m, 8H). ^{13}C NMR, 21,6, 47.9, 48.8, 49.8, 54.4, 127.4, 127.5, 128.9, 129.6, 129.9, 130.0, 134.4, 135.5, 136.6, 143.8, 144.0. MS m/z (FAB) 865 $[M+H]^+$.

$\mathbf{L^1}\cdot 4HBr$

In a round bottom flask were introduced $\mathbf{L^1}$·4Ts (3.0 g, 3.5 mmol), PhOH (16.2 g, 165 mmol) and HBr/AcOH (33%, 166 mL). The solution was stirred under reflux for 18 h to obtain a precipate. This precipitate was filtrated and washed consecutively with CH_2Cl_2 (100 mL) and EtOH (100 mL) to obtain $\mathbf{L^1}$·4HBr as a white solid product (1.5 g, 74% yield): mp 234–238 °C. ^{1}H NMR, 2.94–2.96 (m, 8H), 3.17 (t, 4H, J = 8 Hz), 4.31 (s, 4H), 7.40 (s, 1H), 7.55 (s, 2H), 7.63 (s, 1H). ^{13}C NMR, 42.1, 42.6, 43.8, 50.5, 131.7, 132.0, 132.9, 133.2. Anal Calcd. For $C_{14}H_{28}N_4Br_4$: C, 29.4, H, 4.9, N, 9.8. Found: C, 29.1, H, 4.9, N, 9.5%.

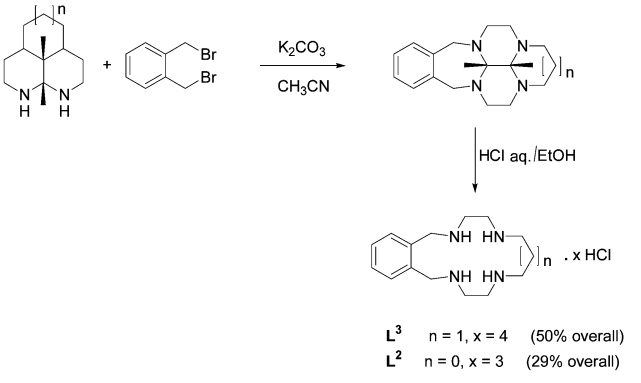

Scheme 1

Synthesis of $\mathbf{L^2}$ and $\mathbf{L^3}$

The ligands $\mathbf{L^2}$ and $\mathbf{L^3}$ were synthesized following the experimental procedure reported in ref. 5 and depicted in Scheme 1. The compounds were isolated and handled as the hydrochloride salts $\mathbf{L^2}$·3HCl and $\mathbf{L^3}$·4HCl and gave satisfactory spectroscopic and elemental analysis. Anal Calcd. for $C_{14}H_{27}N_4Cl_3$($\mathbf{L^2}$·3HCl) C, 47.0, H, 7.6, N, 15.7. Found: C, 46.2, H, 7.6, N, 15.3%. $C_{15}H_{30}N_4Cl_4$($\mathbf{L^3}$·4HCl) C, 44.1, H, 7.4, N, 13.7. Found: C, 43.8, H, 7.3, N, 13.5%.

X-ray crystallography

Crystal data and details of the data collection for the picrate salt $[H_2\mathbf{L^3}](pic)_2{\cdot}1/2C_3H_6O$ (**1**) (pic = 2,4,6-trinitrophenolate) and the complexes $[Cu\mathbf{L^3}Cl](ClO_4)_2$ (**2**) and $[Zn\mathbf{L^3}Cl]Cl{\cdot}H_2O$ (**3**) are given in Table 1†.

For (**1**) the crystal data was collected with an Enraf-Nonius CAD-4 single crystal diffractometer (λ = 0.71073 Å) , and for (**2**) and (**3**) with a Nonius Kappa CCD equipment (λ = 0.71073 Å). The crystals were monitored for decay during data collection and corrections for decay were made, if warranted. Profile analysis was performed on all reflections.[7] A semiempirical absorption correction, Ψ-scan based, was performed .[8] Lorentz and polarisation corrections were applied and the data were reduced to F^2_o values. The structure was solved by the Patterson method using the program SHELXS-86 running on an IBM PENTIUM III 1000 computer.[9] Isotropic least-squares refinement was performed by means of the program SHELXL-93.[10] In the crystallographic analysis of **1**, the protons on the nitrogen atoms in the macrocycle have been located. The other hydrogen atoms of **1** and those of **2** and **3** were placed in calculated positions.

All the non-hydrogen atoms were refined anisotropically. The hydrogen atoms were refined with a common thermal parameter. Atomic scattering factors were taken from the International Tables for X-Ray Crystallography.[11] The molecular plots were produced by the program ORTEP.[12]

$[H_2\mathbf{L^3}](pic)_2\cdot 1/2C_3H_6O$ (1)

Crystals of **1** suitable for X-ray analysis were obtained on crystallisation of **L** dipicrate from an acetone–water mixture. Anal. Calcd. for $C_{28.5}H_{35}N_{10}O_{14.5}$: C, 45.7, H, 4.7, N, 18.7. Found : C, 45.6, H, 4.8, N, 18.9%.

Synthesis of $[Cu\mathbf{L^3}Cl]ClO_4$ (2) and $[Zn\mathbf{L^3}Cl]Cl\cdot H_2O$ (3)

Crystals of **2** and **3** suitable for X-ray analysis were obtained respectively by slow evaporation at pH 8.0 or pH 9.0 of solu-

† CCDC reference numbers 209937–209939. See http://www.rsc.org/suppdata/nj/b3/b303470d/ for crystallographic data in .cif or other electronic format.

Table 1 Crystal data and structure refinement for $[H_2L^3](pic)_2{\cdot}1/2C_3H_6O$ (**1**), $[CuL^3Cl](ClO_4)$ (**2**) and $[ZnL^3Cl]Cl{\cdot}H_2O$ (**3**)

	1	2	3
Empirical formula	$C_{28.5}H_{35}N_{10}O_{14.5}$	$C_{15}H_{26}Cl_2CuN_4O_4$	$C_{15}H_{28}Cl_2ZnN_4O$
Formula weight	749.66	460.84	416.70
Temperature (K)	173(2)	293(2)	293(2)
Wavelength (Å)	0.71073	0.71073	0.71073
Crystal syst	Triclinic	Orthorhombic	Triclinic
Space Group	$P\bar{1}$	P_{mnb}	$P\bar{1}$
a (Å)	8.188(1)	9.4520(2)	7.1050(2)
b (Å)	13.392(2)	11.0000(3)	11.2190(3)
c (Å)	15.778(2)	19.3590(7)	12.2640(4)
α (deg)	92.796(3)		98.202(1)
β (deg)	92.386(3)		95.208(1)
γ (deg)	101.263(3)		92.828(1)
Volume (Å^3)	1692.4(4)	2012.8(1)	961.66(5)
Z	2	4	2
Calculated density (g cm^{-3})	1.471	1.521	1.439
Abs coeff (mm^{-1})	0.120	1.378	1.563
$F(000)$	784	956	436
θq range (degrees)	1.96 to 23.31	2.10 to 27.50	2.88 to 27.49
Reflections collected/unique	7904/4854 [$R(int) = 0.0362$]	4286/2413 [$R(int) = 0.0432$]	6918/4363 [$R(int) = 0.0201$]
Goodness-of-fit on F^2	1.051	1.008	0.877
Final R indices [$I > 2\sigma(I)$]	$R1 = 0.0714$, $wR_2 = 0.2123$	$R_1 = 0.0441$, $wR_2 = 0.1285$	$R_1 = 0.0361$, $wR_2 = 0.1062$
R indices (all data)	$R_1 = 0.0989$, $wR_2 = 0.2435$	$R_1 = 0.1044$, $wR_2 = 0.1758$	$R_1 = 0.0480$, $wR_2 = 0.1169$

$w = 1/[\sigma^2(Fo^2) + (0.2537\ P)^2 + 12.86\ P]$ where $P = (\text{Max}\ (Fo^2) + 2\ Fc^2)/3$.

tions containing $\mathbf{L^2}{\cdot}4HCl$ and $Cu(ClO_4)_2$ or $Zn(ClO_4)_2$ in 1:1 molar ratio. Anal 2. Calcd for $C_{15}H_{26}Cl_2CuN_4O_4$(**1**): C, 39.1, H, 5.7, N, 12.2. Found: C, 39.0, H, 5.5, N, 12.3%. Calcd for $C_{15}H_{28}Cl_2ZnN_4O$ (**2**): C, 43.2, H, 6.8, N, 13.5. Found: C, 43.2, H, 6.5, N, 13.4%. **(CAUTION.** Picrate and perchlorate salts can be explosive and have to be handled with care.)

emf Measurements

The potentiometric titrations were carried out at 298.1 ± 0.1 K using $NaClO_4$ 0.15 mol dm^{-3} as supporting electrolyte. The experimental procedure (burette, potentiometer, cell, stirrer, microcomputer, *etc.*) has been fully described elsewhere.[13] The acquisition of the emf data was performed with the computer program PASAT.[14] The reference electrode was an Ag/AgCl electrode in saturated KCl solution. The glass electrode was calibrated as a hydrogen-ion concentration probe by titration of previously standardized amounts of HCl with CO_2-free NaOH solutions and determining the equivalent point by the Gran's method,[15] which gives the standard potential, $E^{\circ\prime}$, and the ionic product of water ($pK_w = 13.73(1)$).

The computer program HYPERQUAD was used to calculate the protonation and stability constants.[16] The pH range investigated was 2.5–10.5 and the concentration of the metal ions and of the ligands ranged from 1×10^{-3} to 5×10^{-3} mol dm^{-3} with M:L molar ratios varying from 2:1 to 1:2 The different titration curves for each system (at least two) were treated either as a single set or as separated curves without significant variations in the values of the stability constants. Finally, the sets of data were merged together and treated simultaneously to give the final stability constants.

NMR measurements

The ^{1}H and ^{13}C NMR spectra were recorded on Varian UNITY 300 and UNITY 400 spectrometers, operating at 299.95 and 399.95 MHz for ^{1}H and at 75.43 and 100.58 MHz for ^{13}C. The spectra were obtained at room temperature in D_2O or $CDCl_3$ solutions. For the ^{13}C NMR spectra dioxane was used as a reference standard ($\delta = 67.4$ ppm) and for the ^{1}H spectra the solvent signal. Adjustments to the desired pH were made using drops of DCl or NaOD solutions. The pH was calculated from the measured pD values using the correlation, pH = pD − 0.4.[17]

Results and discussion

Acid–base behaviour

Table 2 shows the stepwise protonation constants of the metacyclophane $\mathbf{L^1}$ orthocyclophanes $\mathbf{L^2}$ and $\mathbf{L^3}$, and those previously reported for the paracyclophane derivative **L**.[3]

Both orthocyclophanes present very large constants for the first and second protonation steps while the values of the protonation constants for the third and fourth protonations are very low. As a matter of fact, under our experimental conditions it has not been even possible to determine the values of the constant for the last protonation step that can be estimated to be clearly below 2 logarithmic units.

Table 2 Stepwise protonation constants for the metacyclophane $\mathbf{L^1}$ and orthocyclophanes $\mathbf{L^2}$ and $\mathbf{L^3}$. The corresponding constants for **L** have also been included by means of comparison

Reaction	$\mathbf{L^1}$	$\mathbf{L^2}$	$\mathbf{L^3}$	$\mathbf{L}^c$	$\mathbf{L}^{4d}$	$\mathbf{L}^{5e}$	$\mathbf{L}^{6e}$	$\mathbf{L}^{7e}$
$H + L = HL^a$	9.53(1)[b]	10.38(1)	11.01(3)	9.39(2)	10.35	11.5	10.92	10.64
$H + HL = H_2L$	8.74(1)	9.30(1)	10.88(3)	8.45(2)	9.71	10.5	9.40	9.82
$H + H_2L = H_3L$	5.61(2)	2.96(2)	2.20(7)	5.38(2)	2.05	1.5	4.62	3.5
$H + H_3L = H_4L$	2.77(3)	< 2	< 2	2.51(1)	< 1	0.9	2.00	1.4

[a] Charges omitted for clarity. [b] Values in parentheses are standard deviations in the last significant figure. [c] Taken from ref. 3. [d] Taken from ref. 19. [e] Taken from ref. 18, $I = 0.1$ mol dm^{-3}.

Interestingly enough, the macrocycle presenting the larger constants for the two first protonation stages and the lower constants for the last two is **L**[3], containing a symmetric set of two ethylenic and one propylenic hydrocarbon chains between the nitrogen atoms in the bridge (Chart 1). The behaviour of the metacyclophane **L**[1] is very close to that reported for the analogue paracyclophane **L** and quite different from that of **L**[2] and **L**[3]. **L**[1] shows large values, although much reduced than **L**[2] and **L**[3], for the first two protonation constants, one intermediate value for the third constant and a much smaller value for the fourth protonation which is however, comparable to the one found for the third protonation step of **L**[2] and **L**[3]. Indeed, the values of the protonation constants of the orthocyclophanes are close to those of saturated azacycloalkanes. The dramatic decrease in basicity between the second and third protonation steps of **L**[2] and **L**[3] ($\Delta(\log K_{H_2L/H_3L}) = 6.34$ and 8.68, respectively) lies between those reported for the well-known macrocycles cyclen **L**[4] ($\Delta(\log K_{H_2L/H_3L}) = 7.66$) and cyclam **L**[5] ($\Delta(\log K_{H_2L/H_3L}) = 9.0$) and those of the macrocycles **L**[6] ($\Delta(\log K_{H_2L/H_3L}) = 4.78$) and **L**[7] ($\Delta(\log K_{H_2L/H_3L}) = 6.32$) (Table 2) with the same number of atoms in the ring as **L**[2] and **L**[3] but with a butylene chain instead of the aromatic spacer.[18,19] Actually, molecular modeling calculations as well as the crystal structure of $[H_2L^3](pic)_2 \cdot 1/2C_3H_6O$ denote that, due to the rigidity afforded by the ring, **L**[2] and **L**[3] present closer sizes to those of cyclen and cyclam, respectively, than to those of **L**[6] and **L**[7]. These results reflect the key influence of the size and arrangement of the macrocyclic cavity on determining the distribution of positively charged atoms and thereby, on the basicity of these cyclic polyamines. Nevertheless, just the repulsion between same sign charges is not enough for explaining all the tendencies found and intramolecular hydrogen bonding should also play an important contribution to the large first two protonation constants observed for **L**[2] and **L**[3]. Indeed, the crystal structure of the picrate salt of the diprotonated form of $[H_2L^3]^{2+}$ shows such a formation of a hydrogen bond network between the protonated and non-protonated amino groups (*vide infra*, see Fig. 2B). Analogously, the dramatic drop in basicity between the second and third protonation steps can be probably ascribed among other factors to the disruption of the intramolecular hydrogen bonding formed in the $[H_2L^3]^{2+}$ species. A similar behaviour has been described for cyclam.[20,21]

In order to obtain further information about the protonation pattern of polyamine compounds, ^1H and ^{13}C NMR spectra often provide valuable information. It is well established,[22] that upon protonation, the carbon atoms placed in β-position and the hydrogen nuclei attached to the carbon atom in α-position to the nitrogen undergoing protonation are those exhibiting the largest changes in chemical shifts. For the metacyclophane **L**[1], a plot of the variation in chemical shift of the quaternary aromatic carbon CB1 (Fig. 1), located only in β-position with respect to N1, shows an important upfield shift ($\Delta\delta = 7.8$ ppm) on going from pH 11.0 to 5.0 where the triprotonated species predominate in solution.

Correspondingly, the chemical shift of H1 moves markedly downfield in the same pH range ($\Delta\delta = 0.7$ ppm) (Fig. 1). At lower pH values, in correspondence with the last protonation, the chemical shifts of these signals do not bear further changes while the signals of C4 and H4 shift upfield and downfield respectively. All these data suggest that two out of the three first protonation steps involve the benzylic nitrogen atoms. Similar results have been obtained for the paracyclophane **L**.[2,23] The desolvation produced by the hydrophobic spacer seems to be an important clue for this behaviour.

However, as above noted, the behaviour of the orthocyclophane derivatives is completely different. For example, clear tendencies are not found for the variation of the chemical shift of the CB1 resonance and upfield movements accompany all the protonation steps of **L**. Similar tendencies are observed for the other signals, which show that in the ortho derivatives the protons do not follow any fixed sequence and are shared by the different nitrogens along the protonation process.

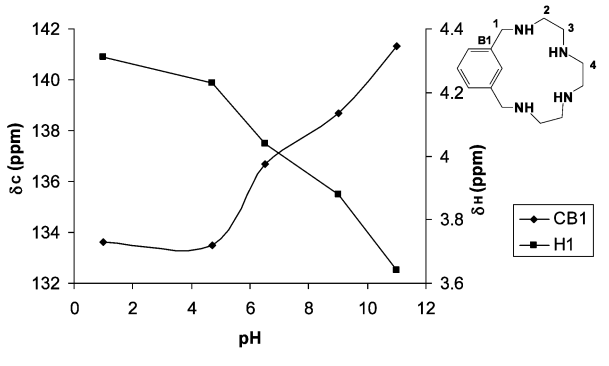

Fig. 1 Representation of the variation of chemical shifts of carbon B1 and hydrogen H1 with the pH for the metacyclophane **L**[1].

Crystal structure of $[H_2L^3](pic)_2 \cdot 1/2C_3H_6O$, 1

Figs. 2A and 2B show the most distinctive features of the crystal structure, which regard the conformation of the macrocycle and the formation of either intramolecular or intermolecular hydrogen bonds. The intramolecular hydrogen bonds are established between alternated protonated and non-protonated amino groups connected by the propylenic chains (Fig. 2B) with distances N1–H···N4 1.946 Å and N3–H···N2 1.797 Å and angles of 166.0 and 166.8°, respectively. This type of intramolecular bonds resemble very much those reported for the perchlorate salt of the diprotonated form of 1,4,8,11-tetraazacycloalkane ($(H_2L^5)^{2+}$, $H_2(cyclam)^{2+}$),[20] although the distances are in the present case shorter. Intermolecular hydrogen bonds occur between the amino groups of **L** and the trinitrophenolate anions.

The bifurcated hydrogen bonds are observed between the phenolate oxygen atoms and the amino groups of the macrocycle with distances N1–H···O1A 2.083 Å, N3–H···O1A 2.166 Å, N2–H···O1B 2.155 Å and N4–H···O1B 2.336 Å and angles of 154, 140, 144, and 128°, respectively. They are ensembled with two weak hydrogen bonds between the protonated amino groups and the nitro groups of the one picrate anion with distances N1–H···O2A 2.362 Å and N3–H···O7A 2.355 Å and angles of 133 and 149°, respectively. One of the picrate anions is placed quite parallel to the benzene ring affording stacking between the rings.

The overall conformation of the macrocycle is folded (Fig. 2) by the effect of the intramolecular hydrogen bonds giving a sort of boat shape to the compound.

Metal coordination

Solution studies

The stepwise stability constants for the formation of Cu^{2+} and Zn^{2+} complexes of the metacyclophane **L**[1] and of the orthocyclophanes **L**[2] and **L**[3] are shown in Tables 3 and 4 conjointly with those for **L**,[2] and relevant data for some saturated tetraazacycloalkanes.[18,24]

The first aspect that deserves comment for the Cu^{2+} complexes is that, accordingly with the protonation behaviour, completely different speciation models are found for the ortho- and meta-derivatives. The model for the systems Cu-**L**[2] and Cu-**L**[3] consists just of the mononuclear species $[CuL^2]^{2+}$, $[CuL^2(OH)]^{3+}$, $[CuHL^3]^{3+}$ and $[CuL^3]^{2+}$, while **L**[1] forms the mononuclear species $[CuH_2L^1]^{4+}$, $[CuHL^1]^{3+}$, $[CuL^1]^{2+}$, $[CuL^1(OH)]^{+}$ and the binuclear ones $[Cu_2L(OH)]^{3+}$ and $[Cu_2L(OH)_2]^{2+}$ (Fig. 3).

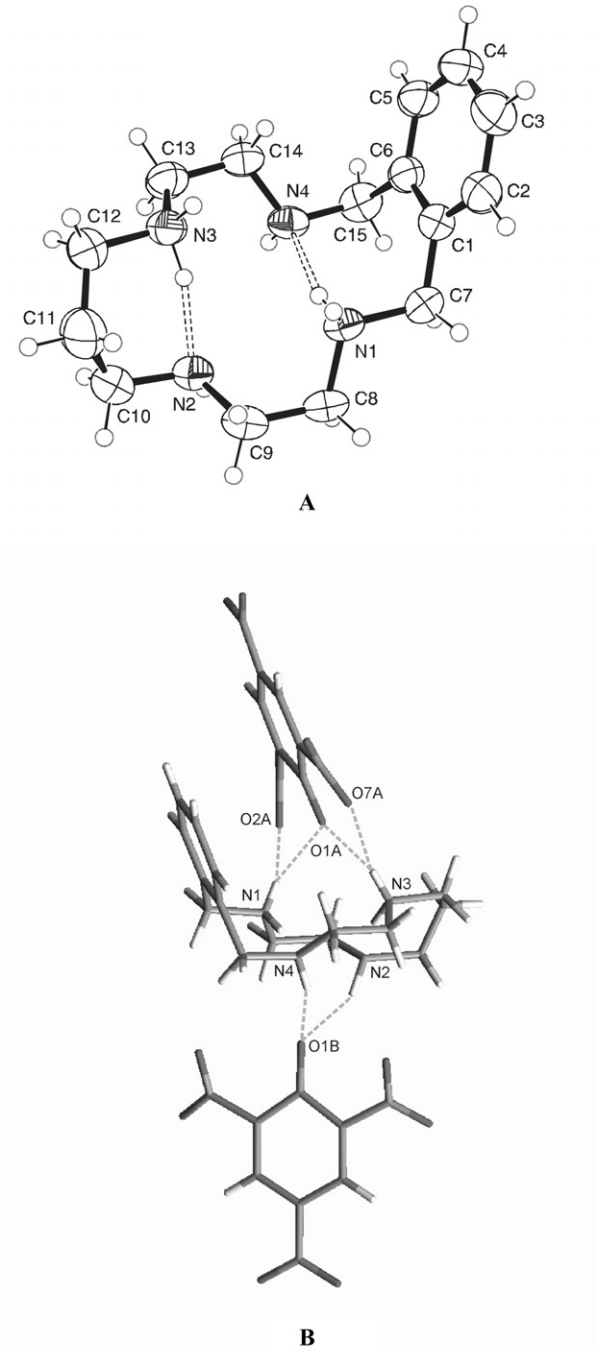

Fig. 2 A) ORTEP plot of the cation $[H_2\mathbf{L}^3]^{2+}$. Counteranions are omitted. Thermal ellipsoids are drawn at the 50% probability level. B) Stick drawing showing inter- and intramolecular hydrogen bonds.

The model found for $\mathbf{L}^1$ keeps some parallelism with that previously reported for the analogue paraazacyclophane **L**. Interestingly enough, the larger meta-derivative 2,6,9,13-tetraaza[14]metacyclophane $\mathbf{L}^8$ with a set of two propylenic and one middle ethylenic chain does not form binuclear complexes.[4]

A second point of interest regards the magnitude of the stability constants of the $[CuL]^{2+}$ and $[ZnL]^{2+}$ complexes, which are much higher for the ortho-derivatives than for the meta-derivatives. In turn, the meta-derivative $\mathbf{L}^1$ presents higher stability than the para-derivative **L** (Tables 3 and 4). On the other hand, the complexes of any of the cyclophane ligands are clearly less stable than those of cyclam and cyclen.

These data can be interpreted taking into account the characteristics of the different ligands here considered. Firstly, at difference with the meta- and para-derivatives, the orthocyclophanes present a suitable size to coordinate a single metal ion involving all their nitrogen donors. Molecular modeling on the free non-protonated **L**, $\mathbf{L}^1$ and $\mathbf{L}^2$ show the distances between the benzylic nitrogens (N1) to be 3.57 Å, 5.34 Å and 6.95 Å, respectively (Chart 2). For **L** the distance between the benzylic nitrogens would be 4.42 Å. The crystal structure of $[H_2\mathbf{L}^3]^{2+}$ shows distances of 2.83 Å between the benzylic nitrogens.

Therefore, para- and meta-substitution prevents both benzylic nitrogens from participating simultaneously in the binding of a single metal ion. This evidence was already provided by several crystal structures involving para-azacyclophanes.[3,4] In the ortho-derivatives, however, the nitrogens can approach close enough to the metal ion for making bonds as denoted by the crystal structures of the complexes $[Cu\mathbf{L}^3Cl]ClO_4$ and $[Zn\mathbf{L}^3Cl]Cl{\cdot}H_2O$ (*vide infra*). Therefore, all four nitrogens of the ortho-derivatives $\mathbf{L}^2$ and $\mathbf{L}^3$ should be involved in the coordination of the metal ions. For $\mathbf{L}^1$, the comparison of the stability constants with those of $\mathbf{L}^2$ and **L** and with relevant data for related systems suggests three as the possible number of co-ordinating nitrogens.

The NMR spectra of a D_2O solution containing zinc triflate and $\mathbf{L}^3$ in molar ratio 1:1 at pH 7 where $[Zn\mathbf{L}^3]^{2+}$ is the only species in solution also support the full-involvement of the nitrogen atoms of **L** in the coordination to Zn^{2+}. The ^{13}C NMR spectrum presents five resonances in the aliphatic region at 21.5, 47.6, 48.8, 49.9 and 51.7 ppm and three signals in the aromatic zone at 129.6 ppm, 132.3 and 136.4 ppm denoting a two-fold symmetry for the complex. The ^1H NMR spectrum at the same pH shows the same symmetry but evidences the stiffening afforded by the metal ion to the molecule. The benzylic protons appear as an AB spin system ($\delta_A = 4.08$ ppm, $\delta_B = 3.56$ ppm, $J_{AB} = 11.2$ Hz). The ethylenic chain and the central propylenic chain present ABCD spin patterns denoting the stiffening that the coordination of the metal imparts to the molecule.

As mentioned above the $[CuL]^{2+}$ complexes of $\mathbf{L}^2$ and $\mathbf{L}^3$ are less stable than the related complexes of cyclen and cyclam. A plausible explanation for this may rest in the 7-membered chelate ring formed at the side of the aromatic ring that

Table 3 Logarithms of the stepwise stability constants for the formation of Cu^{2+} complexes by $\mathbf{L}^1$, $\mathbf{L}^2$ and $\mathbf{L}^3$ determined in 0.15 mol dm^{-3} at 298.1 K. The corresponding constants for the paracyclophane $\mathbf{L}^3$ have also been included by means of comparison

Reaction	$\mathbf{L}^1$	$\mathbf{L}^2$	$\mathbf{L}^3$	$\mathbf{L}^c$	$\mathbf{L}^{4d}$	$\mathbf{L}^{5d}$	$\mathbf{L}^{6d}$
$CuHL + H = CuH_2L^a$	3.58(5)[b]						
$CuL + H = CuHL$	6.90(2)		3.89(5)	6.51			
$Cu + L = CuL$	13.52(4)	19.58(5)	17.73(3)	10.41	24.6	27.2	15.47
$CuL + H_2O = CuL(OH) + H$	−8.82(5)	−11.42(7)		−8.14			
$2Cu + L + H_2O = Cu_2L(OH) + H$	10.67(4)						
$2Cu + L + 2H_2O = Cu_2L(OH)_2 + 2H$	3.60(5)			3.44			

[a] Charges omitted for clarity. [b] Values in parentheses are standard deviations in the last significant figure. [c] Taken from ref. 3. [d] Taken from ref. 18, $I = 0.1$ mol dm^{-3}.

Table 4 Logarithms of the stepwise stability constants for the formation of Zn^{2+} complexes by **L**, $\mathbf{L^2}$ and $\mathbf{L^3}$ determined in 0.15 mol dm^{-3} at 298.1 K. The corresponding constants for the paracyclophane $\mathbf{L^3}$ have also been included by means of comparison

Reaction	$\mathbf{L^1}$	$\mathbf{L^2}$	$\mathbf{L^3}$	$\mathbf{L}^c$	$\mathbf{L}^{4d}$	$\mathbf{L}^{5d}$	$\mathbf{L}^{6d}$
$ZnHL + H = ZnH_2L^a$							
$ZnL + H = ZnHL$	7.08(4)[b]			6.51			
$Zn + L = ZnL$	6.27(3)	13.45(1)	13.77(1)[b]	4.55	16.2	15.5	12.90
$ZnL + H_2O = ZnL(OH) + H$	−7.97(5)	−8.96(2)	−10.33(2)	−8.60	−8.02	−9.77	

[a] Charges omitted for clarity. [b] Values in parentheses are standard deviations in the last significant figure. [c] Taken from ref. 3. [d] Taken from ref. 18, $I = 0.1$ mol dm^{-3}.

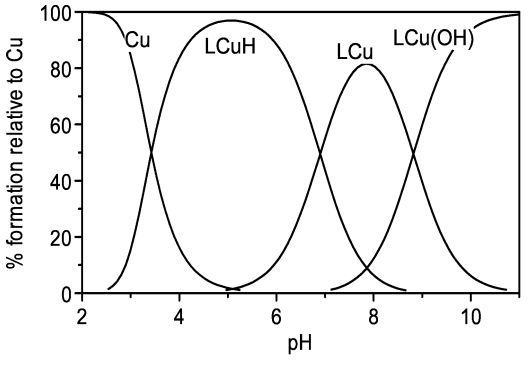

A

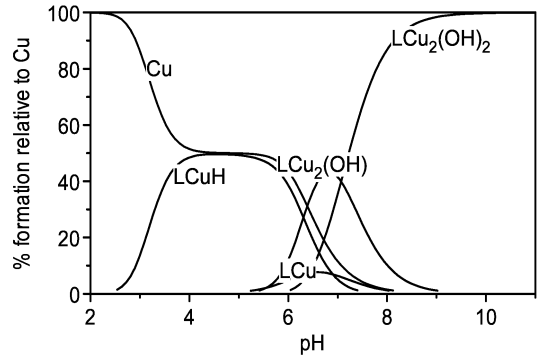

B

Fig. 3 Distribution diagram for the system Cu^{2+}-$\mathbf{L^1}$. A) $[Cu^{2+}] = [\mathbf{L^1}] = 10^{-3}$ M. B) $[Cu^{2+}] = 2 \times 10^{-3}$ M, $[\mathbf{L^1}] = 10^{-3}$ M.

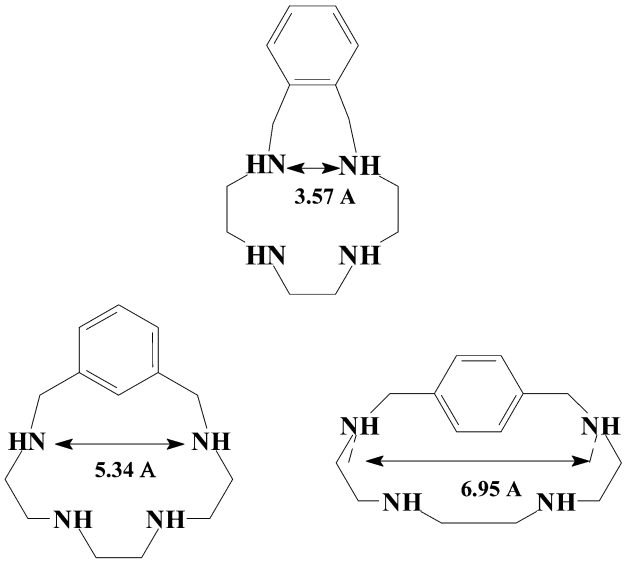

Chart 2

would bear energetically expensive conformational rearrangements for binding the metal. However, the comparison of the stability constants for $\mathbf{L^2}$ and the aza-cycloalkane $\mathbf{L^6}$ with the same number of atoms in the macrocyclic ring denotes in this case an even more energetically demanding situation.[18,25]

Crystal structure of $[CuL^3Cl](ClO_4)$ (2)

The crystal structure of $[CuL^3Cl](ClO_4)$ is a chain-like structure in which $[CuL^3]^{2+}$ fragments are interconnected through asymmetric chloride bridges (Figs. 4A and 4B).

The coordination geometry around the copper is a strongly distorted octahedron. The vertices of the equatorial plane are defined by the nitrogen atoms of the macrocycle with distances Cu1–N4 2.051(4) Å and Cu(1)–N4 2.039(4) Å. The Cu(II) ion is sited in the average plane defined by the four nitrogen atoms. The chloride anions placed at the axial positions connect asymmetrically two metal ion centers (Cu–Cl distances 2.718(2) and 2.810(2) Å). Table 5 collects the distances and angles around the coordination site.

The Cu–N distances are longer than those found in the cationic complex $[Cu(cyclam)]^{2+}$ denoting the steric hindrance provided by the 7-membered chelate ring at the side of the aromatic fragment.[26] The conformation of the five-membered chelate rings is gauche while the six membered-ring presents a chair conformation. An analogous conformation is displayed by the seven-membered ring at the side of the aromatic ring that might be defined as a chair with a back defined by the

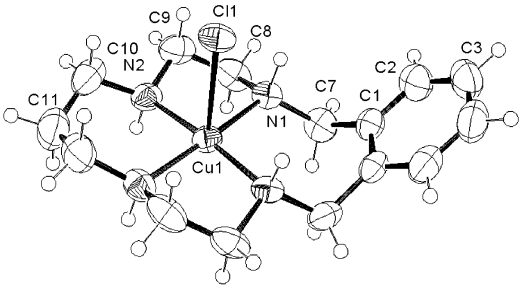

A

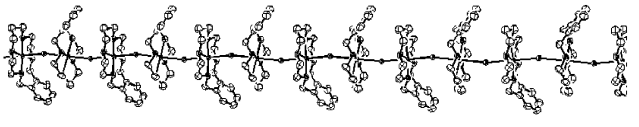

B.

Fig. 4 A) ORTEP drawing for the cation $[CuL^2Cl]^+$. Thermal ellipsoids are drawn at the 50% probability level. B) Portion of one of the chains formed in the crystal structure.

Table 5 Bond angles and distances for $[CuL^3Cl](ClO_4)$ (**2**)

Cu(1)–N(2)	2.036(3)
Cu(1)–N(1)	2.054(3)
Cu(1)–Cl(1)	2.7178(13)
N(2)#1–Cu(1)–N(2)	91.41(19)
N(2)#1–Cu(1)–N(1)	175.80(12)
N(2)–Cu(1)–N(1)	84.83(14)
N(2)–Cu(1)–N(1)#1	175.80(12)
N(1)–Cu(1)–N(1)#1	98.87(17)
N(2)–Cu(1)–Cl(1)	94.46(10)
N(1)–Cu(1)–Cl(1)	87.70(10)

Symmetry transformations used to generate equivalent atoms: #1 −x + 1/2,y,z, #2 −x + 3/2,y,z

Table 6 Selected bond angles and distances for $[ZnL^3Cl]Cl{\cdot}H_2O$ (**3**)

Zn(1)–N(3)	2.129(2)
Zn(1)–N(2)	2.140 (2)
Zn(1)–N(1)	2.144(2)
Zn(1)–N(4)	2.145(2)
Zn(1)–Cl(1)	2.3507(7)
N(3)–Zn(1)–N(2)	87.13(8)
N(3)–Zn(1)–N(1)	160.07(8)
N(2)–Zn(1)–N(1)	82.75(8)
N(3)–Zn(1)–N(4)	83.15(7)
N(2)–Zn(1)–N(4)	161.65(8)
N(1)–Zn(1)–N(4)	101.52(7)
N(3)–Zn(1)–Cl(1)	100.72(6)
N(2)–Zn(1)–Cl(1)	98.21(6)
N(1)–Zn(1)–Cl(1)	97.70(6)
N(4)–Zn(1)–Cl(1)	98.87(5)

aromatic carbon atoms (see Fig. 4A). The disposition of the hydrogen atoms of the nitrogen donors is ++−− following the notation that Bosnich *et al* have introduced for related chelates,[27] and the folding of he ligand will define a trans IIII RRSS isomer.[28]

Crystal structure of $[ZnL^3Cl]Cl \cdot H_2O$ (3)

The crystal structure consists of $[ZnL^2Cl]^+$ cations and chloride counteranions. The coordination geometry around the Zn^{2+} metal ion is a square pyramid with the nitrogen atoms occupying the vertices of the square and one chloride anion placed in apical position. The mean distance Zn–N is *ca.* 2.14 Å and the distance Zn–Cl 2.3507(7) Å (Fig. 5, Table 6). At difference with the structure of the Cu^{2+} complex, in this case the chloride anions do not interconnect different macrocyclic units.

The conformations of the different chelate rings around the Zn^{2+} metal ions are similar to those described for the Cu^{2+} complexes with gauche disposition for the five-membered rings, and chair and chair-like conformation for the six- and seven-membered chelate rings.

The folding of the macrocycle defines again a trans IIII, RRSS conformational isomer. The angle formed between the plane defined by the aromatic ring and the mean plane passing through the nitrogen donors is of *ca.* 30°. Interestingly enough this angles rises when passing to the meta and para-derivatives. For this last one, the disposition would be almost normal.

Conclusions

The results presented provide a general and conclusive view of how topologically simple ligands containing a benzene ring linked to the ends of tetraaminic chains through benzylic positions can achieve different coordination modes depending on the substitution of the aromatic spacer and on the length of hydrocarbon chain between the nitrogen atoms. While the ortho-derivatives just form mononuclear complexes, in the case of the meta- and para-derivatives the right selection of the hydrocarbon spacers in the tetraaminic chains may yield the formation of coordinatively unsaturated binuclear complexes.

These characteristics are currently being explored from the point of view of recognition of different substrates as tertiary ligands through formation of mixed complexes and from the point of view of assisting different catalytic processes.

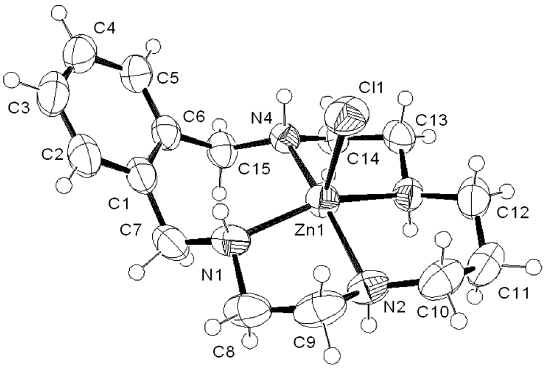

Fig. 5 ORTEP drawing for the cation $[ZnL^3Cl]^+$. Thermal ellipsoids are drawn at the 50% probability level.

Acknowledgements

We would like to acknowledge Ministerio de Ciencia y Tecnología BQU2000-1424 and Academy of Sciences (project Z4055905) and Grant Agency of the Czech Republic (203/98/0726, 203/01/0067) for financial support.

References

1 W. Kaim, B. Schwederski, *Bioinorganic Chemistry: Inorganic Elements in the Chemistry of Life, An Introduction and Guide*, J. Wiley & Sons, Chichester, 1995; E. Solomon, T. C. Brunold, M. I. Davis, J. N. Kemsley, S.-K. Lee, N. Lehnert, F. Neese, A. J. Skulan, Y.-S. Yang and J. Zhou, *Chem. Rev.*, 2000, **100**, 235.

2 D. E. Fenton, *Chem. Soc. Rev.*, 1999, **28**, 159; Y. Murakami, J.-I. Kikuchi, Y. Hisaeda and O. Hayashida, *Chem. Rev.*, 1996, **96**, 721; R. Breslow and S. D. Dong, *Chem. Rev.*, 1999, **98**, 1997; N. Kitajima and W. B. Tolman, *Prog. Inorg. Chem.*, 1995, **43**, 419; J. H. Hartley, T. D. James and C. J. Ward, *J. Chem. Soc., Perkin Trans.*, 2000, **1**, 3155; E. Kimura, T. Koike, M. Shionaya and M. Shiro, *Chem. Lett.*, 1992, 787; A. Bencini, E. Berni, A. Bianchi, V. Fedi, C. Giorgi, P. Paoletti and B. Valtancoli, *Inorg. Chem.*, 1999, **38**, 6323.

3 A. Andrés, C. Bazzicalupi, A. Bianchi, E. García-España, S. V. Luis, J. F. Miravet and J. A. Ramírez, *J. Chem. Soc.,Dalton Trans.*, 1994, 1995.

4 A. Andrés, M. I. Burguete, E. García-España, S. V. Luis, J. F. Miravet and C. Soriano, *J. Chem. Soc., Perkin Trans.*, 1993, **2**, 749; A. Doménech, J. V. Folgado, E. García-España, S. V. Luis, J.-M. Llinares, J. F. Miravet and J. A. Ramírez, *J. Chem. Soc., Dalton Trans.*, 1995, 541; E. García-España, J. Latorre, S. V. Luis, J. F. Miravet, P. Pozuelo, J. A. Ramírez and C. Soriano, *Inorg. Chem.*, 1996, **35**, 4591; B. Altava, M. I. Burguete, S. V. Luis, J. F. Miravet, E. García-España, V. Marcelino and C. Soriano, *Tetrahedron*, 1997, **53**, 4751; D. K. Chand, H.-J. Schneider, J. A. Aguilar, F. Escartí, E. García-España and S. V. Luis, *Inorg. Chim. Acta*, 2000, **316**, 71.

5 M. Chadim, M. Budesinsky, J. Hodacova and J. Zavada, *Collect. Czech. Chem. Commun.*, 2000, **65**, 99.

6 A. Bencini, M. I. Burguete, E. García-España, S. V. Luis, J. F. Miravet and C. Soriano, *J. Org. Chem.*, 1993, **58**, 4749.

7 (*a*) M. S. Lehman and F. K Larsen, *Acta Crystallogr.*, 114, **11**, Sect.A 1978; (*b*) D. F. Grant and E. F. Gabe, *J. Appl. Crystallogr. Sect A*, 1978, **11**, 114.
8 A. C. T Nort, D. C. Philips and F. S. Mathews, *Acta Crystallogr. Sect. A*, 1968, **24**, 351.
9 G. M. Sheldrick, C. Kruger, R. Goddard, ed., *Crystallographic Computing*, Clarendon Press, Oxford, England, 1985, p. 175.
10 G. M. Sheldrick, SHELXL-93, *Program for Crystal Structure Refinement*, University of Göttingen, Germany, 1993.
11 *International Tables for X-ray Crystallography*, The Kynoch Press, Birmingham, England, 1974, vol. IV.
12 C. K. Johnson, ORTEP; Report ORNL- 3794; Oak Ridge National Laboratory, Oak Ridge, TN, 1971.
13 E. García-España, M.-J. Ballester, F. Lloret, J.-M. Moratal, J. Faus and A. Bianchi, *J. Chem. Soc., Dalton Trans.*, 1988, 101.
14 M. Fontanelli and M. Micheloni, *Proceedings of the I Spanish-Italian Congress on Thermodynamics of Metal Complexes*, Diputación de Castellón, Castellón, Spain, 1990 Program for the automatic control of the microburette and the acquisition of the electromotive force readings.
15 G. Gran, *Analyst (London)*, 1952, **77**, 881; F. J. Rossotti and H. Rossotti, *J. Chem. Educ.*, 1965, **42**, 375.
16 P. Gans, A. Sabatini and A. Vacca, *Talanta*, 1996, **43**, 1739.
17 A. K. Convington, M. Paabo, R. A. Robinson and R. G. Bates, *Anal. Chem.*, 1968, **40**, 700.
18 A. E. Martell, R. M. Smith and R. J. Moteikaitis, *NIST Critical Stability Constants, of Metal Complexes Database NIST Standard Reference Database*, Version 4, 1997.
19 A. Bencini, A. Bianchi, E. García-España, M. Micheloni and J. A. Ramírez, *Coord. Chem. Rev.*, 1999, **88**, 97.
20 C. Nave and M. Truter, *J. Chem. Soc., Dalton Trans*, 1974, 2351.
21 M. Studer, A. Riesen and T. A. Kaden, *Helv. Chim. Acta*, 1989, **72**, 1253.
22 J. E. Sarnesky, H. L. Surprenant, F. K. Molen and C. N. Reiley, *Anal. Chem.*, 1975, **47**, 2116.
23 A. Bianchi, B. Escuder, E. García-España, S. V. Luis, V. Marcelino, J. F. Miravet and J. A. Ramírez, *J. Chem. Soc., Perkin Trans.*, 1994, **2**, 1253.
24 R. M. Izatt, K. Pawlak and J. S. Bradshaw, *Chem. Rev.*, 1991, **91**, 1721.
25 A. Bianchi, L. Bologni, P. Dapporto, M. Micheloni and P. Paoletti, *Inorg. Chem.*, 1984, **23**, 1201.
26 P. A. Tasker and L. Sklar, *J. Cryst. Mol. Struct.*, 1975, **5**, 329.
27 B. Bosnich, C. K. Poon and M. L. Tobe, *Inorg. Chem.*, 1965, **4**, 1102.
28 E. K. Barefield, A. Bianchi, E. J. Billo, P. J. Connolly, P. Paoletti, J. S. Summers and D. G. . Van der Derveer, *Inorg. Chem.*, 1986, **25**, 4197 and references therein.